

RESEARCH ARTICLE

Structural Basis for the Inhibition of a Phospholipase A₂-Like Toxin by Caffeic and Aristolochic Acids

Carlos A. H. Fernandes^{1,2}, Fábio Florença Cardoso^{1,2,3}, Walter G. L. Cavalcante^{1,2,3}, Andreimar M. Soares^{4,5}, Maeli Dal-Pai⁶, Marcia Gallacci³, Marcos R. M. Fontes^{1,2*}

1 Dep. de Física e Biofísica, Instituto de Biociências, UNESP—Universidade Estadual Paulista, Botucatu, São Paulo, Brazil, **2** Instituto Nacional de Ciência e Tecnologia em Toxinas, CNPq, São Paulo, São Paulo, Brazil, **3** Dep. de Farmacologia, Instituto de Biociências, UNESP—Universidade Estadual Paulista, Botucatu, São Paulo, Brazil, **4** Fundação Oswaldo Cruz (FIOCRUZ), Porto Velho, Rondônia, Brazil, **5** Centro de Estudos de Biomoléculas Aplicadas, Universidade Federal de Rondônia, Porto Velho, Rondônia, Brazil, **6** Dep. de Morfologia, Instituto de Biociências, UNESP—Universidade Estadual Paulista, Botucatu, São Paulo, Brazil

* fontes@ibb.unesp.br



OPEN ACCESS

Citation: Fernandes CAH, Cardoso FF, Cavalcante WGL, Soares AM, Dal-Pai M, Gallacci M, et al. (2015) Structural Basis for the Inhibition of a Phospholipase A₂-Like Toxin by Caffeic and Aristolochic Acids. PLoS ONE 10(7): e0133370. doi:10.1371/journal.pone.0133370

Editor: Israel Silman, Weizmann Institute of Science, ISRAEL

Received: May 30, 2015

Accepted: June 25, 2015

Published: July 20, 2015

Copyright: © 2015 Fernandes et al. This is an open access article distributed under the terms of the [Creative Commons Attribution License](https://creativecommons.org/licenses/by/4.0/), which permits unrestricted use, distribution, and reproduction in any medium, provided the original author and source are credited.

Data Availability Statement: The coordinates were deposited in the Protein Data Bank (PDB) under the identification codes 4YZ7 (PrTX-I/AA) and 4YU7 (PrTX-I/CA).

Funding: Support was provided by Fundação de Amparo à Pesquisa do Estado de São Paulo (FAPESP) to CAHF, FFC, WGLC, MDP, MRMF; Conselho Nacional de Desenvolvimento Científico e Tecnológico (CNPq) to MDP, AMS, MRMF and Coordenação de Aperfeiçoamento de Pessoal de Nível Superior (CAPES) to MRMF.

Abstract

One of the main challenges in toxicology today is to develop therapeutic alternatives for the treatment of snake venom injuries that are not efficiently neutralized by conventional serum therapy. Venom phospholipases A₂ (PLA₂s) and PLA₂-like proteins play a fundamental role in skeletal muscle necrosis, which can result in permanent sequelae and disability. This leads to economic and social problems, especially in developing countries. In this work, we performed structural and functional studies with Piratoxin-I, a Lys49-PLA₂ from *Bothrops spirajai* venom, complexed with two compounds present in several plants used in folk medicine against snakebites. These ligands partially neutralized the myotoxic activity of PrTX-I towards binding on the two independent sites of interaction between Lys49-PLA₂ and muscle membrane. Our results corroborate the previously proposed mechanism of action of PLA₂s-like and provide insights for the design of structure-based inhibitors that could prevent the permanent injuries caused by these proteins in snakebite victims.

Introduction

In Asia, Africa and Latin America, approximately 98% of the world's snakebites occur, with 421,000 envenomations and 20,000 deaths by ophidian accidents [1]. However, these numbers may be as high as 1,841,000 envenomations and 94,000 deaths per year, considering the under-reporting that occurs in these regions [1]. The mortality caused by snakebites is higher than several neglected tropical diseases, including dengue hemorrhagic fever, leishmaniasis, cholera, schistosomiasis and Chagas disease [2]. Consequently, the World Health Organization (WHO) recognizes snakebites as an important neglected tropical disease.

Competing Interests: The authors have declared that no competing interests exist.

In Latin America, snakes of the *Bothrops* genus are responsible for approximately 80% of all ophidian accidents [3,4]. Envenomation by these snakes is associated with prominent local tissue damage characterized by swelling, blistering, hemorrhaging and necrosis of the skeletal muscle. These effects are not efficiently neutralized by conventional serum therapy and can result in permanent sequelae and disability [5,6]. The main toxins involved in tissue-damaging activities are the phospholipases A₂ (PLA₂s) and metalloproteinases, which are the most abundant components of venoms from the *Bothrops* genus [7]. A subgroup of PLA₂s, known as PLA₂-like proteins, is catalytically inactive due to lack of Ca²⁺ coordination related to natural mutations of its primary structure; however, it is still able to induce a drastic local myonecrosis [8–10]. The most studied PLA₂-like proteins are the Lys49-PLA₂s, in which the mutations Asp49→Lys and Tyr28→Asn impair the Ca²⁺ coordination [11,12]. Several studies with Lys49-PLA₂s have shown that segment 115–129 of the C-terminal region, which includes a variable combination of positively charged and hydrophobic residues, is responsible for the myotoxic activity of these proteins [13–16]. Recently, a mechanism of action has been proposed for the Lys49-PLA₂s and all other PLA₂-like proteins that includes a quaternary conformational change for the activation of these proteins and the participation of two independent interaction sites with the membrane [17,18].

In folk medicine, especially in developing countries, several vegetal species are employed for the treatment of ophidian envenomations in communities that lack prompt access to serum therapy [19,20]. In recent years, some studies have investigated the effects of plants on snake-bites, including the isolation and characterization of their active constituents and the elucidation of their possible mechanisms of action [19,21–23].

Aristolochic acid (AA) and caffeic acid (CA) are plant compounds with anti-snake venom properties that are used in folk medicine [19–21]. AA (8-methoxy-6-nitrophenanthro (3,4-d-1,3-dioxole-5-carboxylic acid) is an alkaloid found in several *Aristolochia* species. This plant is among the most popular anti-snake venom folk compounds able to neutralize rattlesnake venom activity [20]. AA causes a dose-dependent inhibition of *in vitro* phospholipid hydrolysis by human synovial fluid PLA₂ and snake venom PLA₂s [24–27]. CA (3-(3,4-dihydroxyphenyl) 2-propenoic acid) is a cinnamic acid derivative, abundant in nature and with exceptional biochemical reactivity. It has a large variety of potential pharmacological effects, such as anti-oxidant, anti-cancer and anti-viral activities [28–30]. CA is found in *Vernonia condensata* leaves, showing antidote activity against *Bothrops jararacavenom* [19,21]. Additionally, crystalline CA derivatives have been demonstrated to be an antidote against snake venom by oral or parenteral administration [31].

In this work, we report functional (neuromuscular-blocking and muscle-damage activities) and crystallographic experiments aiming to study the possible inhibitory effects of AA and CA on PrTX-I, a Lys49-PLA₂ isolated from *Bothrops spirajai* snake venom. Our functional studies indicate that these ligands neutralize the myotoxic activity of PrTX-I but do not present effect on the inhibition of neuromuscular blocking activity. The structural studies demonstrated that both ligands interact with PrTX-I in different regions, corroborating the previously proposed myotoxic mechanism for PLA₂-like proteins.

Material and Methods

Protein Purification and Inhibitor Source

PrTX-I was isolated from *Bothrops spirajai* snake venom by gel filtration and ion exchange chromatography techniques, as previously described [32]. Aristolochic acid (AA) and caffeic acid (CA) were purchased from Sigma-Aldrich (St Louis, MO, USA).

Functional Studies

Animals. Institutional Animal Care and Use Committee (Institute of Biosciences–Sao Paulo State University–UNESP) approved this study under the number 033/05. Animal procedures were in accordance with the guidelines for animal care prepared by the Committee on Care and Use of Labor. Adult male mice weighing 25–30g were maintained under a 12 h light-dark cycle in a temperature-controlled environment ($22\pm 2^\circ\text{C}$) for at least 10 days prior to the experiments, with food and water *ad libitum*.

Neuromuscular-blocking activity. Mice were euthanized by cervical dislocation followed by exsanguination. The phrenic nerve-diaphragm muscle preparation was removed and mounted vertically in a conventional isolated organ-bath chamber containing 15 mL of Ringer's physiological solution of the following composition (mM): NaCl, 135; KCl, 5; MgCl₂, 1; CaCl₂, 2; NaHCO₃, 15; Na₂HPO₄, 1; glucose, 11. This solution was bubbled with carbogen (95% O₂ and 5% CO₂). The preparation was attached to an isometric force transducer (Grass, FT03) to record the twitch tension. The transducer signal output was amplified and recorded on a computer via a transducer signal conditioner (Gould, 13-6615-50) with an AcquireLab Data Acquisition System (Gould). The resting tension was 5 g. Indirect contractions were evoked by supramaximal pulses (0.2 Hz, 0.5 ms) delivered from an electronic stimulator (Grass, S88K) and applied to the phrenic nerve by means of a suction electrode.

The preparation was stabilized for 45 minutes before the addition of a single concentration of toxin. For inhibition experiments, a fixed amount of PrTX-I dissolved in Ringer's physiological solution was mixed with AA and CA to obtain a 1:1 and 1:5 (w/w) toxin/inhibitor ratio. At molar ratio terms, it means 1:40 and 1:76 for 1:1 (w/w) toxin/inhibitor ratio for AA and CA, respectively, and 1:200 and 1:380 for 1:5 (w/w) ratio. The mixtures were incubated for 30 minutes at $35\pm 2^\circ\text{C}$. The control experiments were performed in the absence of toxin or in the presence of inhibitors alone. The degree of protection offered by AA and CA after 90 minutes of contact with the preparation was expressed as a percentage of neuromuscular blockade observed in the presence of the mixture of toxin plus inhibitor relative to the blockade observed in the presence of toxin alone.

Muscle-damage activity. After the myographic study, the diaphragm muscle was removed from the bath and immersed in Bouin's fixative, and then processed and embedded in Historesin (Kit Historesin Leica). Histological transverse sections (5 mm thick) were cut out in a microtome and stained with hematoxylin and eosin (HE) prior to examination by light microscopy [33]. Morphological damage was quantified in HE-stained preparations using an Imaging Analysis System (Leica, Qwin). The number of fibers with lesions was expressed as a percentage of the total number of cells (muscle damage index) in three non-overlapping non-adjacent areas of each muscle observed at the same magnification. The degree of neutralization offered by AA and CA was expressed as a percentage of the muscle damage index in the presence of the toxin plus inhibitor relative to that index in the presence of the toxin alone.

Statistical analysis. The data are expressed as the mean \pm S.E.M. The statistical analysis of the data was carried out using ANOVA complemented by the Tukey-Kramer test. Values of $P < 0.05$ were considered significant.

Structural studies

Crystallization of the complexes PrTX-I/AA and PrTX-I/CA. Co-crystallization experiments were performed with PrTX-I at a concentration of $12 \text{ mg}\cdot\text{mL}^{-1}$. Crystals of the complexes were obtained by the hanging drop method [34]. AA and CA were dissolved in ultrapure water or 50% (w/v) ethanol, respectively, to give an 8:1 molar ratio of inhibitor:protein in the crystallization drops. The drops consisted of 1 μL protein solution,

0.2 μ L inhibitor solution and 0.8 μ L reservoir solution and were equilibrated against 500 μ L of the same reservoir solution. The best crystals were obtained after an optimization process for the native protein crystallization conditions [35]; the reservoir solution consisted of 26–30% polyethylene glycol 4000 (PEG 4000), 100 mM Tris-HCl pH 8.1–8.5 and 200 mM lithium sulfate, as previously described for the PrTX-I/CA complex [36]. Crystals were grown at 291 K for approximately four weeks for both protein complexes.

X-ray data collection and processing. The X-ray diffraction data for all crystals were collected at a wavelength of 1.45 Å using a synchrotron-radiation source (MX2 station, Laboratório Nacional de Luz Síncrotron, LNLS, Campinas, Brazil) and a MAR CCD imaging-plate detector (MAR Research). Crystals were mounted in nylon loops and flash-cooled in a stream of nitrogen gas at 100 K using no cryoprotectant. The data were processed using the HKL program package [37].

Structure determination and refinement. The crystal structures were determined by molecular replacement techniques implemented in the program MOLREP [38] from the CCP4i program package [39] using the coordinates from the crystal structures of the PrTX-I-complexed with α -tocopherol (PDB ID 3CYL) [35] and both prothostoxin-I (BthTX-I), and a Lys49-PLA₂ isolated from *Bothrops jararacussu* venom complexed with PEG 4000 (PDB ID 3IQ3) [12] as models for the PrTX-I/AA and PrTX-I/CA complexes, respectively. The modeling processes were always performed by manual rebuilding with the program Coot [40] using electron density maps calculated with the coefficients $2|F_{\text{obs}}| - |F_{\text{calc}}|$. The models were improved, as judged by the free R-factor [41], through rounds of crystallographic refinement (positional and restrained isotropic individual B-factor refinement, with an overall anisotropic temperature factor and bulk solvent correction) using PHENIX [42]. In the structure of the PrTX-I/AA complex, due to a lack of electron density, part or full side chains of the following residues were excluded: Leu2 (monomer A), Phe3 (monomers A and B), Lys7(A,B), Lys11(A), Lys15 (A,B), Lys20(A), Val31(A), Leu32(A,B), Lys36(A,B), Arg43(A), Lys53(A,B), Lys57(A,B), Lys69(A,B), Lys70(A,B), Arg72(A,B), Lys78(A,B), Asp79(A), Asn88(A), Glu94(B), Lys115(A), Lys116(A), Lys122(A), Phe125 (A,B), Lys127(A,B), Lys129(B), and Asp130(A). In the structure of the PrTX-I/CA complex, part or full side chains of the following residues were excluded: Phe3(A), Leu32(B), Lys36(A), Lys53(B), Lys57(A,B), Thr59(A), Lys69(A,B), Lys70(A,B), Lys78(A), Lys127(B), and Lys129(A). The stereochemical qualities of the models were determined with the PHENIX and MolProbity programs [42,43].

Results

Neuromuscular blocking activity

PrTX-I (1.0 μ M) promoted a time-dependent blockade of indirectly evoked twitches in mice phrenic-diaphragm preparations. After 90 minutes, the twitch amplitudes were reduced to 89.4% (Fig 1). The paralyzing effect of PrTX-I could not be reversed by washing the preparation for at least 30 minutes with toxin-free physiological solution (data not shown). The mean time required to reduce the twitch amplitudes by 50% ($T_{1/2}$) was 34.0 ± 2.4 minutes. Pre-incubation with CA (1:1 and 1:5 w/w) or AA (1:1 and 1:5 w/w) did not prevent the neuromuscular blockade induced by PrTX-I (Fig 1A and 1B). Alone, CA did not affect the twitch amplitude (Fig 1A), while AA (68.5 μ g/mL) promoted a facilitator effect (Fig 1B).

Muscle-damaging activity

Light microscopy showed that control and CA or AA-treated muscles were of normal appearance. Fibers were delimited by a thin layer of connective tissue (endomysium) and presented a polygonal shape, with an acidophilic sarcoplasm and peripheral nuclei (Fig 2A, 2C, 2E, 2G and

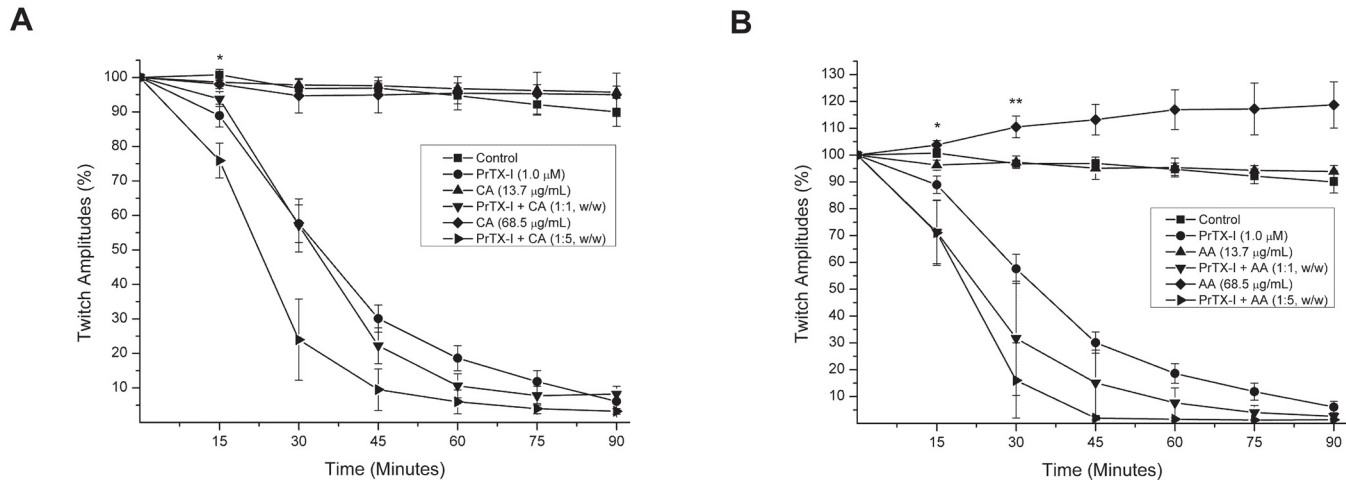


Fig 1. Effects of PrTX-I and PrTX-I pre-incubated with caffeic acid [CA](A) and aristolochic acid [AA] (B) on indirectly evoked twitches in mouse phrenic-diaphragm preparations. The ordinate represents the percentage amplitude of twitches relative to the initial amplitude. The abscissa indicates the time from the beginning of each treatment in the organ bath. The points are the mean \pm S.E. * indicates the point at which differences between PrTX-I treatments (alone and pre-incubated with CA and AA) and the control become significant. ** indicates the point at which differences between AA (68.5 μ g/mL) and the control become significant.

doi:10.1371/journal.pone.0133370.g001

2I). A few fibers from muscles exposed to AA (13.7 μ g/mL and 68.5 μ g/mL) revealed a loss of myofibrils (Fig 2G and 2I). However, as shown in Fig 3, only muscles exposed to AA (68.5 μ g/mL) had a significant muscle damage index compared to the control ($6.8 \pm 2.9\%$, $n = 3$ vs. $1.2 \pm 0.1\%$, $n = 4$). After 90 minutes of contact with PrTX-I, the diaphragm muscle showed several changes, such as round fibers and edema. Many fibers presented cytoplasm areas devoid of myofibrils, some with a central nucleus (Fig 2B). The muscle damage index for the PrTX-I group was significantly higher than the control ($35.1 \pm 0.7\%$, $n = 4$ vs. $1.2 \pm 0.1\%$, $n = 4$) (Fig 3). In contrast, pre-incubation with CA (13.7 μ g/mL and 68.5 μ g/mL) or AA (13.7 μ g/mL) reduced the myotoxic effects of PrTX-I. In fact, diaphragm muscles exposed to the pre-incubation product presented a more conserved aspect (Fig 2D, 2F and 2H). The muscle damage indices of these preparations were $22.0 \pm 3.5\%$ and $12.7 \pm 1.9\%$ (PrTX-I/CA at ratios of 1:1 and 1:5, respectively) and $20.2 \pm 0.9\%$ (PrTX-I/AA at 1:1) (Fig 3). On the other hand, the pre-incubation of AA with PrTX-I at the ratio 1:5 (w/w) did not reduce the muscle damage index when compared to PrTX-I alone ($33.8 \pm 0.7\%$, $n = 3$ vs. $35.1 \pm 0.7\%$, $n = 4$) (Fig 2J).

Overall crystallographic structures

Crystals of both complexes diffracted at high resolution (Table 1) and classified as belonging to the P₂₁2₁2 or P₂₁ space groups for PrTX-I/AA and PrTX-I/CA, respectively. The refinements converged to final R values of 17.3% (R_{free} = 23.5%) and 18.3% (R_{free} = 22.9%), respectively, for PrTX-I/AA and PrTX-I/CA. The final models (Fig 4) are of a stereochemical quality expected for structures with the same resolution, as indicated by r.m.s.d bonds, r.m.s.d. angles and Ramachandran plot analyses (Table 1). Both structures have seven disulfide bridges in each monomer with the following structural features: (i) an N-terminal α -helix; (ii) a “short” helix; (iii) a Ca²⁺ binding loop; (iv) two anti-parallel α -helices (2 and 3); (v) two short strands of an anti-parallel β -sheet (β -wing); and (vi) a C-terminal loop (Fig 4), similar to all other class II PLA₂s [44,45].

The inspection of the $2|F_{obs}| - |F_{calc}|$ electronic density map of the PrTX-I/CA structure revealed the presence of four CA molecules establishing hydrogen bonds in monomer A with

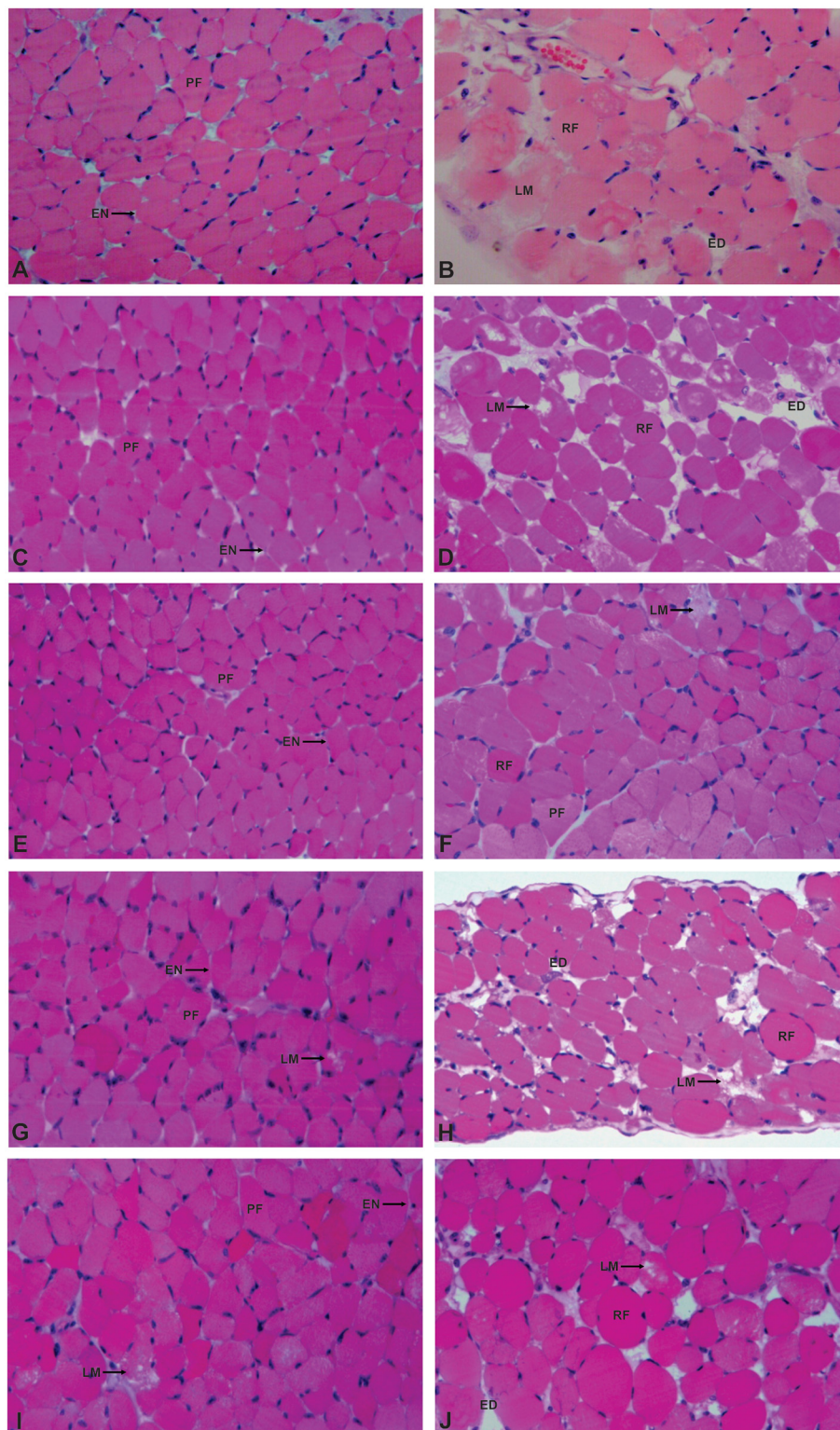


Fig 2. Light micrographs of mouse diaphragm muscles submitted to hematoxylin and eosin staining. Control muscle (A) and muscle exposed to caffeic acid (CA) and aristolochic acid (AA) (C, E, G and I) show fibers with normal appearance as evidenced by the polygonal aspect of fibers (PF) and endomysium (EN). A few fibers present loss of myofibrils in the muscle exposed to AA (G and I). (B) Muscle exposed to PrTX-I: edema (ED), round fibers (RF), some of which present loss of myofibrils (LM). (D, F, H and J) Muscle

exposed to PrTX-I pre-incubated with CA and AA: The fibers have characteristics observed less frequently in the fibers treated with the PrTX-I alone, except in J, which occurred at similar frequencies.

doi:10.1371/journal.pone.0133370.g002

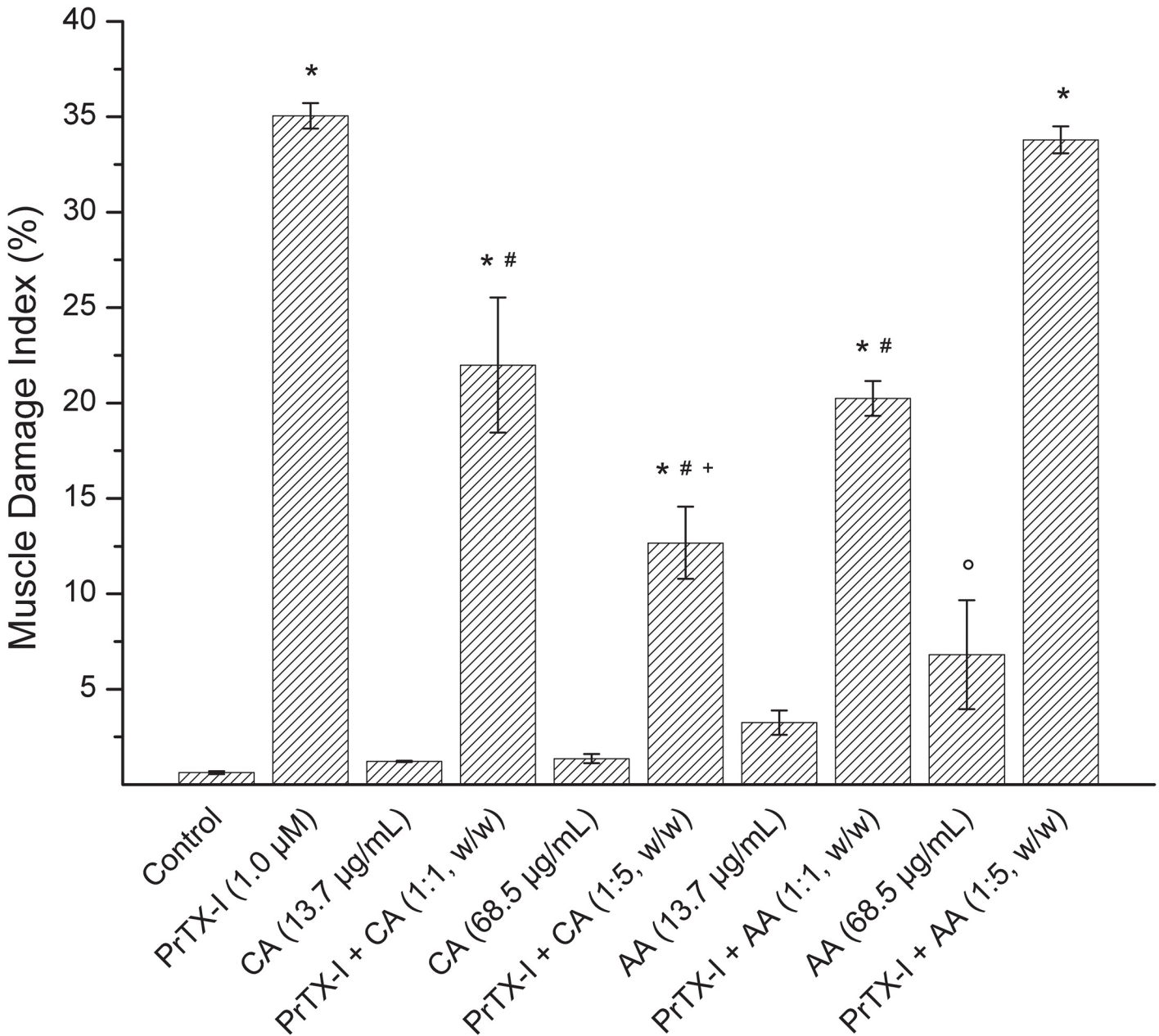


Fig 3. Effect of CA and AA upon the muscle damage index induced by PrTX-I in mouse diaphragm preparations. The ordinate represents the percentage of damaged fibers relative to normal fibers and the abscissa indicates the experimental groups. The bars are expressed as the mean ± S.E. * indicates when differences between PrTX-I treatments (alone and pre-incubated with CA or AA) and their respective controls was significant. # indicates when there were significant differences between PrTX-I pre-incubated with inhibitors and PrTX-I alone treatments. + indicates significant differences between PrTX-I treatments pre-incubated with CA. ° indicates significant differences between the AA (68.5 μg/mL) treatment and the Control group.

doi:10.1371/journal.pone.0133370.g003

Table 1. X-ray data collection and refinement statistics.

	PrTX-I-Aristolochic Acid	PrTX-I-Caffeic Acid
Unit Cell (Å)	a = 68.3; b = 70.9; c = 44.0	a = 39.2; b = 72.8; c = 44.6; β = 102.1°
Space Group	P2 ₁ 2 ₁ 2	P2 ₁
Resolution (Å)	25.61–1.96 (2.03–1.96) ^a	37.34–1.65 (1.70–1.65) ^a
Unique reflections	15848 (1541) ^a	27814 (2724) ^a
Completeness (%)	99.22 (98.59) ^a	94.47 (92.59) ^a
R _{merge} ^b	6.3 (49.0) ^a	6.5 (39.5) ^a
Mean I/σ (I)	14.33 (2.02) ^a	27.4(2.34) ^a
R _{cryst} ^c (%)	17.30	18.23
R _{free} ^d (%)	23.52	22.87
Number of non-hydrogen atoms ^e		
Protein	1749	1849
Ligands	60	108
Waters	174	289
RMS (bonds) ^e	0.007	0.008
RMS (angles) ^e	1.14	1.18
Average B-factor (Å ²) ^e		
Protein	29.60	32.10
Ligands	54.40	56.40
Solvent	37.10	40.60
Ramachandran favored (%) ^e	98	95
Ramachandran outliers (%) ^e	0	0
Clashscore ^f	4.77	11.37
MolProbity Overall Score ^f	1.54	1.78

^a Numbers in parenthesis are for the highest resolution shell.

^b $R_{merge} = \sum_{hkl} (\sum_i (|I_{hkl,i} - \langle I_{hkl} \rangle|)) / \sum_{hkl} \langle I_{hkl} \rangle$, where $I_{hkl,i}$ is the intensity of an individual measurement of the reflection with Miller indices h, k and l, and $\langle I_{hkl} \rangle$ is the mean intensity of that reflection. Calculated for $I > -3\sigma(I)$.

^c $R_{cryst} = \sum_{hkl} (|F_{obs,hkl}| - |F_{calc,hkl}|) / |F_{obs,hkl}|$, where $|F_{obs,hkl}|$ and $|F_{calc,hkl}|$ are the observed and calculated structure factor amplitudes, respectively.

^d R_{free} is equivalent to R_{cryst} but calculated with reflections (5%) omitted from the refinement.

^e Calculated with Phenix [42].

^f Calculated with MolProbity [43].

doi:10.1371/journal.pone.0133370.t001

Lys15 and Arg118 and by water molecules with Ile82 and Lys100 (Fig 5). In monomer B, CA molecules establish hydrogen bonds with Lys20 and Arg118 by water molecules with Gly15, Asn17 and Ser21 (Fig 5). Moreover, CA molecules establish hydrophobic contacts with Lys20, Lys115, Ile104, Arg107, Glu108 and Leu121 in monomer A and with Lys15, Lys20 and Lys115 in monomer B (Fig 6). In other Lys49-PLA₂s crystal structures, sulfate ions were found interacting with most of the residues that establish contacts with CA on the PrTX-I/CA structure [18,35]. However, it is possible to determine, by checking electron density omit-maps, an unambiguous interpretation of CA for these maps (Fig 5). Moreover, CA molecules modeled on these maps presented lower mean B-factor values (55.7 Å²) when compared with sulfate ions modeled on the same region (88.9 Å²). For comparison reason, sulfate ions modeled in the same region for other Lys49-PLA₂s structures presented following B-factor values: 44.2 Å² in PrTX-I/αT (PDB ID 3CYL); 68.8 Å² in BthTX-I/αT (PDB ID 3CXI); and 52.9 Å² in MTX-II/PEG4K (PDB ID 4K06).

In addition, three PEG 4000 molecules were noted in the PrTX-I/CA structure, with two PEGs inside the hydrophobic channels from both monomers and the third PEG

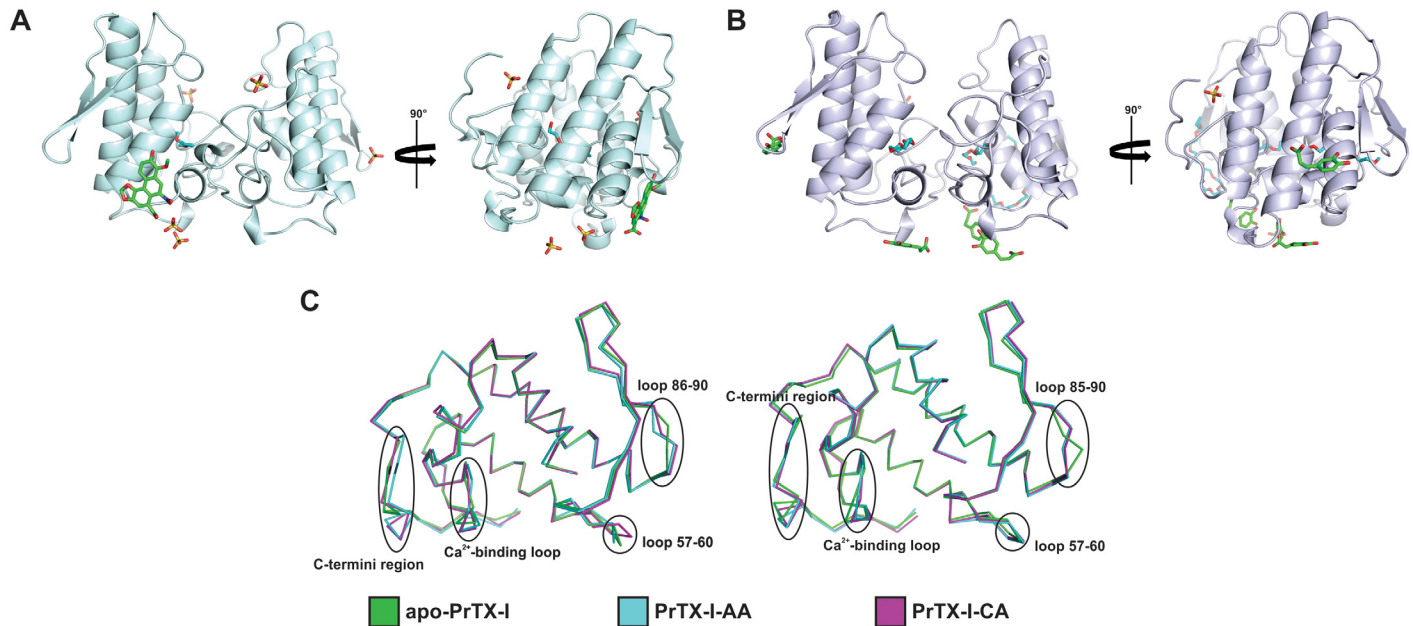


Fig 4. Dimeric structures of (A) PrTX-I complexed to aristolochic acid (PrTX-I/AA) and (B) PrTX-I complexed to caffeic acid (PrTX-I/CA) shown as a cartoon representation. PEG molecules, sulfate ions, AA and CA are indicated by sticks (in cyan, yellow, blue and green, respectively). In yellow sticks are also highlighted the aminoacids that compose MDiS (Leu121) and MDoS (Lys20, Lys155, Arg118) regions, which interact with AA and CA, respectively. (C) C α superposition of apo-PrTX-I, PrTX-I/AA, PrTX-I/CA and PrTX-I complexed to rosmarinic acid (PrTX-I/RA) (monomers A and B, respectively) highlighting the most important structural deviations between them.

doi:10.1371/journal.pone.0133370.g004

molecule interacting with Lys7 on monomer B. The PEG molecules found in these sites are found in other Lys49-PLA₂s structures [12,18,46]. Finally, in the PrTX-I/CA structure, a sulfate molecule established hydrogen bonds with Arg33 in monomer A, similarly to sulfate ions found in other Lys49-PLA₂s structures [18,35].

On the other hand, in the PrTX-I/AA structure just one AA molecule was observed which established hydrogen bonds with N-terminal residues from monomer B (Gly15 and Asn17 by two water molecules) in close proximity to the C-terminal region from monomer A, especially Leu121 (Fig 5). Moreover, AA established hydrophobic contacts with Leu121 and Pro123 from monomer A and with Lys7, Gln11 and Leu10 from monomer B (Fig 6). Furthermore, five sulfate ions interacted with several basic residues of the PrTX-I/AA structure (Lys20, Arg34, Lys115 and Arg118), similarly to that observed in other Lys49-PLA₂s structures. Finally, a part of a PEG 4000 molecule (nine atoms in the electron density map) inside the monomer B hydrophobic channel was noted.

Structural comparison between apo-PrTX-I and complexes with PrTX-I crystal structures

Superposition among the complexed structures PrTX-I/AA, PrTX-I/CA and PrTX-I rosmarinic acid (PrTX-I/RA) [47] resulted in a C α atom r.m.s. deviation in the range of 0.3–0.4 Å. In contrast, a similar superposition between the complexed structures and the apo structure had an r.m.s.d. close to 1.0 Å (Table 2). These values are comparable to other Lys49-PLA₂s [35,48], where a pattern was observed among apo forms with an r.m.s.d. of approximately 1.0 Å, while for structures that present with molecules in the hydrophobic channel (e.g., PEG and α -tocopherol) these values are significantly lower. These higher values for apo forms occur mainly due to differences in their C-termini, demonstrating the higher conformational flexibility of

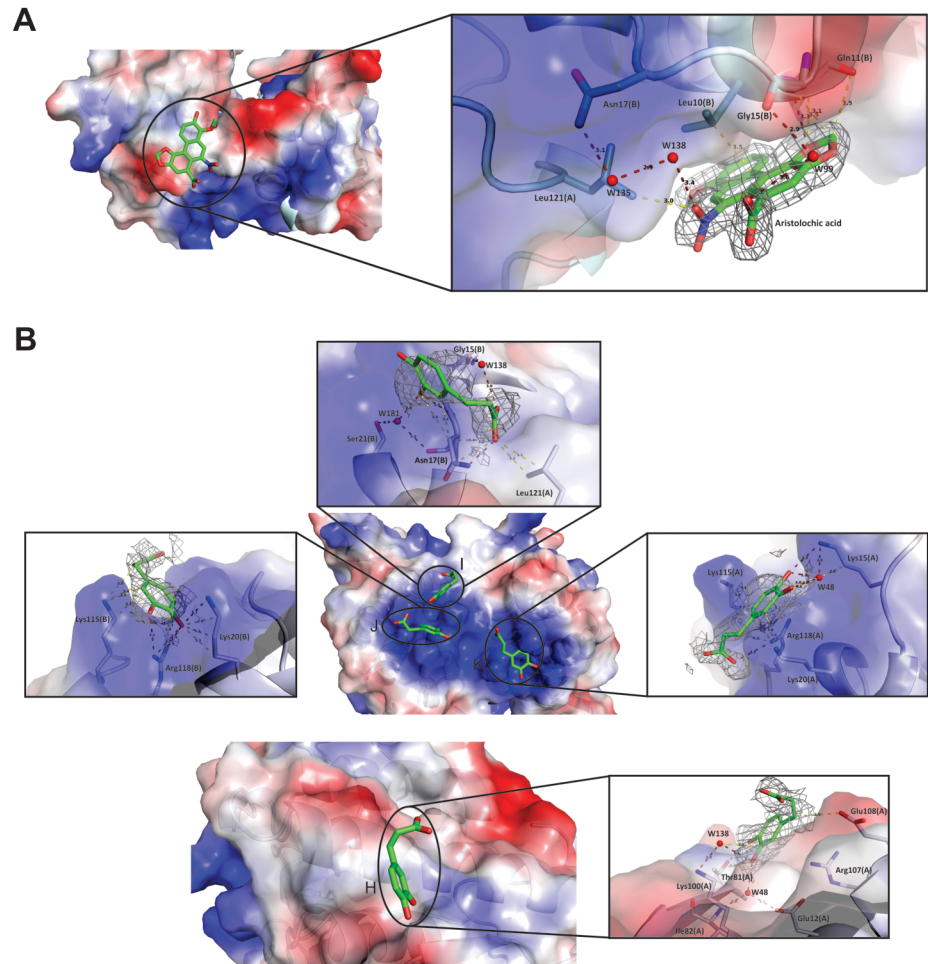


Fig 5. Electrostatic potential surface of (A) PrTX-I complexed to aristolochic acid (PrTX-I/AA) and (B) PrTX-I complexed to caffeic acid (PrTX-I/CA) crystal structures. The distances (Å) between protein inhibitors are shown as yellow dashes for bump distances and red dashes for hydrogen bond distances. Residues of monomers A and B in contact with AA and CA are represented by sticks. Omit electron density maps for AA and CA molecules (gray meshes) were calculated with the coefficients $2|F_{obs}| - |F_{calc}|$ contoured at 1.0 standard deviation.

doi:10.1371/journal.pone.0133370.g005

this region. The main differences occur in three regions of each monomer: Ca²⁺ binding loop (residues 29–34), the loop after the β -wing (residues 85–90) and in the C-termini (117–130) (Fig 4). These differences are observed on several Lys49-PLA₂s superpositions [12,18] and thus, the ligands do not cause relevant changes in the tertiary structure conformation of the protein.

Regarding the quaternary structure, PrTX-I structures complexed to AA, CA or RA have two protomers in the asymmetric unit (Fig 4) and present similar oligomeric structures. As observed for other bothropic Lys49-PLA₂s [35], there are two choices of dimeric structure in their unit cells. However, there are several examples of experimental and functional data for this class of proteins showing that the oligomeric conformation known as the “alternative dimer” is the most likely to occur in solution (for a review refer to [17]). Then, both PrTX-I structures were refined on this oligomeric conformation. In structures that present molecules in a hydrophobic channel solved in an alternative dimer conformation, it was observed that a Tyr119:Tyr119 interchain hydrogen bond is formed between the monomers [35]. This interaction was also observed for the complexed PrTX-I structures (AA, CA or RA) because these

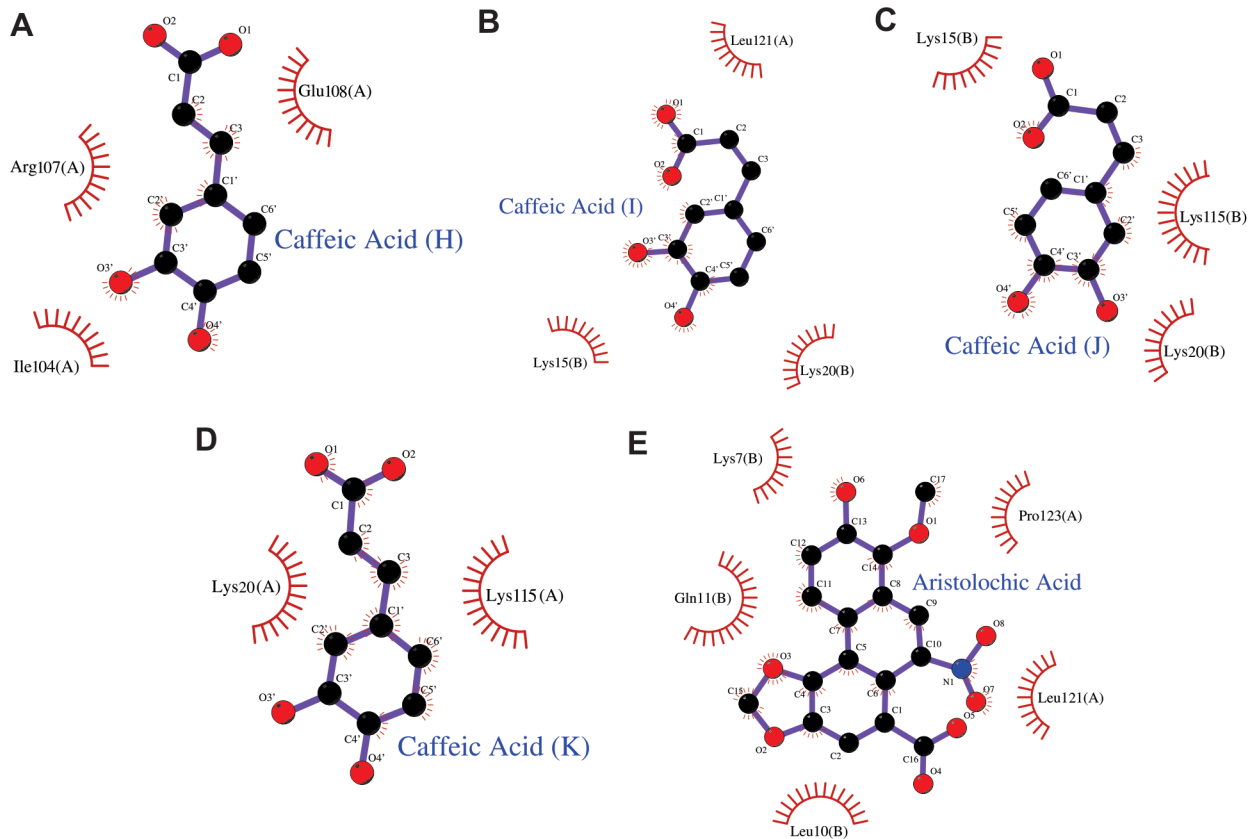


Fig 6. Hydrophobic contacts between caffeic acid (A, B, C and D) and aristolochic acid (E) molecules with PrTX-I observed in crystal structures. Drawn using Ligplot[60].

doi:10.1371/journal.pone.0133370.g006

structures present PEG molecules in their hydrophobic channels. According to Fernandes and colleagues [18], PLA₂-like structures with molecules at the hydrophobic channel are in their active state because the entrance of a molecule in this channel leads to a quaternary conformational change. This conformational change constitutes the first step of mechanism of action of these proteins [18]. In addition, this phenomenon can be measured by the “two-angle model” previously proposed, which reflects the aperture and torsion of the dimer after molecular binding on hydrophobic channel [35]. PrTX-I/AA, PrTX-I/CA and PrTX-I/RA have 40°, 39° and 43° torsion angles and 27°, 28° and 23° aperture angles, respectively. These values are in

Table 2. Superposition between protomers of apo-PrTX-I, PrTX-I complexed to Aristolochic Acid (PrTX-I/AA), PrTX-I complexed to Caffeic Acid (PrTX-I/CA) and PrTX-I complexed to Rosmarinic Acid (PrTX-I/RA) crystallographic structures (r.m.s. deviations (Å) of C_α atoms).

		apo-PrTX-I	
		Monomer A	Monomer B
PrTX-I/AA	Monomer A	0.82	0.41
	Monomer B	0.83	0.49
PrTX-I/CA	Monomer A	0.79	0.56
	Monomer B	0.83	0.58
PrTX-I/RA	Monomer A	1.04	0.55
	Monomer B	0.98	0.59

doi:10.1371/journal.pone.0133370.t002

agreement with structures in the active state [35,48]. In contrast, inactive (or apo) structures have higher values of torsion angles (60°-61°) and smaller values of aperture angles (6°-7°) [35,48].

Discussion

The plant-derived molecules caffeic and aristolochic acids inhibit PrTX-I myotoxic activity

Several groups of indigenous people use specific plant extracts against snakebites, and the identification of their active compounds is an active field of study. Recently, some studies showed that several constituents of these plant extracts contain anti-snake venom properties [19,21–23]. Recently, structural and functional studies demonstrated that rosmarinic acid (RA) was able to inhibit the *invitro* paralyzing activity caused by PrTX-I in mice neuromuscular preparations by 80% [47]. In addition, light and electron micrographs of mouse diaphragm muscle also demonstrated that PrTX-I may severely damage muscle fibers [47,49]. On the other hand, preparations exposed to PrTX-I that were pre-incubated with RA presented fibers with normal aspects [47].

In this study, both caffeic (CA) and aristolochic acids (AA) partially neutralized the muscle damage promoted by PrTX-I. As CA is a RA precursor, it was expected that its inhibitory activities against PrTX-I effects would be similar in the phrenic-diaphragm preparation. However, CA was ineffective at inhibiting the *invitro* paralyzing activity of this toxin. On the other hand, light microscopy analysis of muscle preparations submitted to myographic experiments showed that CA protected against the myotoxic effect induced by PrTX-I by 40% and 65% (PrTX-I/CA at ratios of 1:1 and 1:5, respectively). The different results between the CA and RA treatments probably was due to distinct interaction sites of these ligands with PrTX-I (see next two sections for more detailed discussion about ligands binding). Similarly to CA, AA did not inhibit the neuromuscular blockade induced by PrTX-I. At a higher concentration (68.5 µg/mL), AA alone promoted negative effects on the phrenic-diaphragm preparation, where it caused twitches facilitated by an unknown mechanism. In addition, there were injured fibers in these preparations, which may explain the high muscle damage index when the PrTX-I/AA ratio was 1:5. Interestingly, at low concentrations (13.7 µg/mL), there was no such damage and AA promoted a partial protection (43%) to myotoxicity induced by the toxin (morphological analysis). Except for the intrinsic toxic effect of AA on the neuromuscular preparation, the toxin neutralization by AA and CA was similar, even though they interact in different regions of PrTX-I.

The paralyzing and muscle damage activities promoted by myotoxic Lys49-PLA₂s, represented here by PrTX-I, were due to their ability to alter the integrity of muscle cell membranes (for a review see [50]). After the initial binding, these myotoxins interact with sarcolemma and promote its destabilization, altering the permeability to ions (Na⁺, K⁺, Cl⁻ and Ca²⁺) and macromolecules [8,50–53]. The first consequence of the ionic collapse is the cell depolarization and the lack of excitability due to the inactivation of voltage-dependent Na⁺-channels, thus impairing the generation of the action potential along the muscle fibers and determining the muscle paralysis. The continuous depolarization surrounding the endplate also reaches the motor nerve terminal, reducing the magnitude of the nerve action potential and consequently the acetylcholine (ACh) release, contributing to muscle paralysis [50, 54, 55]. Another consequence of the cell depolarization is the release of Ca²⁺ from intracellular pools [56], starting several deleterious effects, such as myofilament hypercontraction, mitochondrial damage and activation of Ca²⁺-dependent proteases and phospholipases [8,51,52], which culminates in the muscle injury [53,57].

Although the paralysis and the muscle fiber damage induced by Lys49-PLA₂s are triggered by alterations in membrane permeability, the contractile process is more sensitive to such action because of its dependence on the cell excitability. Thus, ligands that partially inhibit the Lys49-PLA₂ actions on cell membrane, such as CA and AA, promotes a partial protection of myotoxicity (up to 65% and 43%, respectively) with no positive interference on muscle paralysis. Corroborating this hypothesis, we have previously demonstrated that ligands able to promote a more effective binding to Lys49-PLA₂, as rosmarinic acid, efficiently prevent both effects[47].

Aristolochic and caffeic acids bind to different regions of PrTX-I and cause myotoxic inhibition by two different mechanisms

Recently, Fernandes and coworkers[18] proposed an action mechanism for Lys49-PLA₂s composed of five steps, which includes an allosteric transition and two independent sites of interaction with the target membrane: i) a cationic membrane docking site (MDoS), composed of the basic residues (usually Lys20, Lys115 and Arg118) responsible for the anchorage of the protein on membrane and ii) a hydrophobic membrane disruption site (MDiS) composed of hydrophobic residues exposed to solvent (Leu121 and Phe125) responsible for the disruption of the membrane.

Interestingly, in this study, we demonstrated that both ligands (AA and CA) are bound to residues related to MDoS and MDiS regions of the toxin and this fact may explain their inhibitory characteristics. In the PrTX-I/CA crystal structure, four CA molecules interact with the protein. Two of them interact with Lys20, Lys115 and Arg118 residues for both monomers by hydrogen bonds and hydrophobic interactions (Figs 5 and 6). In other Lys49-PLA₂ crystal structures, it is common to observe sulfate ions, which arise from the crystallization conditions, establishing similar contacts with these residues[18,35]. Based on analysis of sulfate positions in PLA₂ crystallographic structures, Bahnson *et al*[58] hypothesized that sulfate ions may simulate the anion head of the phospholipid, revealing putative regions of the protein that could interact with the target membrane. This observation led Santos and colleagues[35] to propose a similar hypothesis for Lys49-PLA₂s, which was corroborated by Fernandes and colleagues[18], who called this region the MDoS. Therefore, these data indicate that CA molecules inhibit PrTX-I myotoxic activity due to their interaction with the MDoS region and consequently avoid the docking of the toxin with the membrane. Regarding the other CA molecules, an interaction with Gly15, Asn17, Ser21 and Leu121 residues close to the MDiS region was observed, suggesting that this CA molecule may also bind to the membrane disruption site of PrTX-I. The fourth CA molecule interacts with Lys100 and Glu108 residues but no function has been assigned to these residues; thus, the binding of this molecule can be attributed to a non-specific interaction.

The crystal structure of PrTX-I/AA reveals an aristolochic acid molecule interacting by hydrogen bonds with Gly15(B) and via water molecules with Asn17(B) and Gln11(B) (Fig 5). This ligand also interacts with the N-terminal portion of monomer B (Lys7, Leu10 and Gln11) and the C-terminus of monomer A (Pro123), which is near the MDiS region (particularly Leu121). Therefore, based on this structural information, we propose that the inhibitory feature observed for this ligand is due to the physical obstruction of the MDiS region that impairs the disruption of the target membrane by the toxin.

The crystal structure of a catalytic PLA₂ (an Asp49-PLA₂) from *Viperarussellii* venom complexed to aristolochic acid was also solved[27]. Interestingly, this ligand binds in a different region compared to PrTX-I and the catalytic inhibition observed for this protein has a different structural basis. In the case of the structure from *V.russelli*, the ligand is located at the hydrophobic channel of the protein, establishing hydrogen bonds with His48 and Asp49 and closing the

entrance of its hydrophobic channel [27]. The explanation for these binding differences between catalytic and non-catalytic PLA₂s is probably the specific amino acid differences between them because these proteins present a high level of secondary and tertiary structural conservation.

In conclusion, the data presented here demonstrate for the first time the occurrence of two independent sites of interaction between a protein and a membrane target, which contributes to the validation of the proposed myotoxic mechanism [17,18].

How can we effectively inhibit bothropic Lys49-PLA₂s?

One of the main challenges in toxicology today is to develop therapeutic alternatives to the treatment of snake venom injuries that are not efficiently neutralized by conventional serum therapy. In the case of Latin American snakes, the local myonecrosis caused by PLA₂ and PLA₂-like proteins is the main consequence of their envenomation [55]. This effect is poorly neutralized by anti-venom administration and, in many cases, may lead to injury, including amputation and permanent disability [5,6]. Therefore, it is important to understand the structural basis of local myonecrosis and to create molecular models that can guide the design of efficient inhibitors that could be used to complement conventional serum therapy. Furthermore, these models also could be used to develop new inhibitors for human PLA₂s, which are involved in several inflammatory processes and present a very conserved tertiary structure in comparison to snake venom PLA₂s [44].

In this work, we performed structural and functional approaches to provide substantial information about the inhibition of myotoxic Lys49-PLA₂s using aristolochic and caffeic acids as molecular models. Taking into account the data presented here and previous studies reported in the literature with other ligands, we propose three different means to inhibit the myotoxicity caused by these proteins:

1. physical blocking for phospholipid binding at the hydrophobic channel of the toxin. There are two different ways to achieve this blocking: a) by binding to the putative "active site" region (His48 residue) (e.g., pBPB) [59], b) by preventing its occupation (e.g., rosmarinic acid) [47];
2. obstruction of the protein-membrane docking region (MDoS) (e.g., caffeic acid);
3. obstruction of the protein region related to membrane destabilization (MDiS) (e.g., aristolochic acid).

AA and CA ligands provided relevant structural information about Lys49-PLA₂s inhibition towards partial neutralization of the myotoxic activity of these proteins. These ligands experimentally highlighted the previously proposed mechanism of action of Lys49-PLA₂s, binding with the two interaction sites of these proteins with the target membrane (MDoS and MDiS) [18]. However, it is important to note that AA and CA ligands do not inhibit neuromuscular blocking activity. In contrast, RA efficiently inhibits the neuromuscular blocking activity (~90%) and neutralizes approximately ~80% of the myotoxic activity of PrTX-I [47]. The analysis of crystal structure from PrTX-I/RA shows that RA causes the physical blocking of lysophospholipid-binding at the hydrophobic channel, in contrast to PrTX-I/AA and PrTX-I/CA structures, where the hydrophobic channel is completely empty (Fig 7). C^α superimposition between PrTX-I/AA, PrTX-I/CA and PrTX-I/RA structures shows that, in fact, AA, CA and RA bind in different regions of the protein (Fig 7). Furthermore, this superimposition also shows that RA causes the blocking of hydrophobic channel because a catechol group of RA occupies the same region of part of the PEG molecule in hydrophobic channel present in

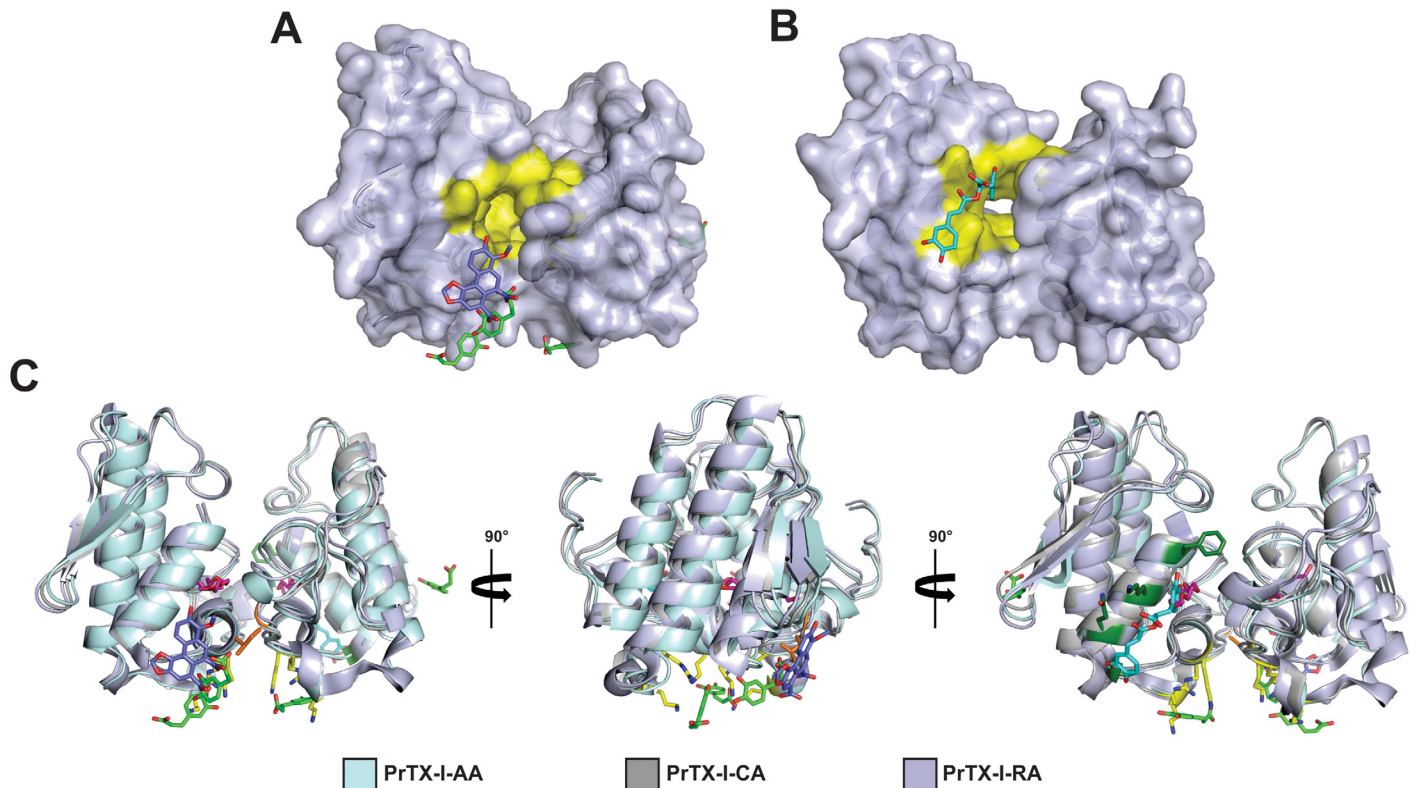


Fig 7. Molecular surface of the PrTX-I complexed to aristolochic acid (PrTX-I/AA) and PrTX-I complexed to caffeic acid (PrTX-I/CA) structures (A) and PrTX-I complexed to rosmarinic acid (PrTX-I/RA) crystal structure (B). PrTX-I/AA and PrTX-I/CA were superimposed using their C^α atoms. The region that composes the hydrophobic channel are highlighted in yellow on molecular surfaces. (C) Structural comparison of binding mode of AA, CA, and RA on the PrTX-I structure. PrTX-I/AA, PrTX-I/CA and PrTX-I/RA were superimposed using their C^α atoms. AA, CA, RA and PEG are highlighted in blue, green, cyan and magenta sticks, respectively. The amino acids that compose MDiS (Leu 121, in orange sticks), MDoS (Lys20, Lys115 and Arg118, in yellow sticks) and hydrophobic channel (Phe3, Lys7, Gln11 and Gly15, in green olive sticks) which interact with AA, CA and RA, respectively, are also highlighted.

doi:10.1371/journal.pone.0133370.g007

PrTX-I/AA and PrTX-I/CA structures (Fig 7). Therefore, we can hypothesize that an inhibitor such as RA, which is able to prevent the allosteric transition, aids more efficiently than a ligand (such as AA and CA) that blockades the MDoS and MDiS regions. These data support the observation that the binding of AA or CA only can occur efficiently after the allosteric transition, when the MDoS and MDiS regions are exposed to the solvent, with the protein in its active state and able to cause membrane lesion.

The results presented here can promote the design of more accurate structure-based inhibitors that, to cause a full inhibition of Lys49-PLA₂s activity could obstruct both the hydrophobic channel and the MDoS and MDiS regions. The putative drug formed by different inhibitors could obstruct all of these regions simultaneously. Finally, it is important to note that other PLA₂s-like proteins (e.g., Arg49 and Ser49-PLA₂s) also have a hydrophobic channel and analogous MDoS and MDiS regions [17]. Consequently, the studies performed here may also be useful to study inhibition methods for these proteins and, consequently, provide an integrated inhibition mechanism for the entire PLA₂-like protein class.

Atomic Coordinates

The coordinates were deposited in the Protein Data Bank (PDB) under the identification codes 4YZ7 (PrTX-I/AA) and 4YU7 (PrTX-I/CA).

Acknowledgments

We also acknowledge the use of the Laboratório Nacional de Luz Síncrotron (LNLS, Brazil).

Author Contributions

Conceived and designed the experiments: CAHF WGLC AMS MG MRMF. Performed the experiments: CAHF FFC WGLC AMS. Analyzed the data: CAHF FFC WGLC AMS MDP MG MRMF. Contributed reagents/materials/analysis tools: AMS MDP MG MRMF. Wrote the paper: CAHF FFC WGLC MG MRMF.

References

1. Kasturiratne A, Wickremasinghe AR, de Silva N, Gunawardena NK, Pathmeswaran A, Premaratna R, et al. (2008) The global burden of snakebite: a literature analysis and modelling based on regional estimates of envenoming and deaths. *PLoS Med* 5: e218. doi: [10.1371/journal.pmed.0050218](https://doi.org/10.1371/journal.pmed.0050218) PMID: [18986210](https://pubmed.ncbi.nlm.nih.gov/18986210/)
2. Harrison RA, Hargreaves A, Wagstaff SC, Faragher B, Laloo DG (2009) Snake envenoming: a disease of poverty. *PLoS Negl Trop Dis* 3: e569. doi: [10.1371/journal.pntd.0000569](https://doi.org/10.1371/journal.pntd.0000569) PMID: [20027216](https://pubmed.ncbi.nlm.nih.gov/20027216/)
3. Saúde FN (2001) Manual de Diagnóstico e Tratamento de Acidentes por Animais Peçonhentos. Brasília: MS/FUNASA.
4. Araújo FAA, Santalúcia M, Cabra RF (2003) Epidemiologia dos acidentes por animais peçonhentos. In: Cardoso JLC, França FOS, Wen FH, Málaque CMS, Haddad Jr, editors. *Animais Peçonhentos no Brasil*. São Paulo: Sarvier. pp. 6–12.
5. Gutierrez JM, Theakston RD, Warrell DA (2006) Confronting the neglected problem of snake bite envenoming: the need for a global partnership. *PLoS Med* 3: e150. PMID: [16729843](https://pubmed.ncbi.nlm.nih.gov/16729843/)
6. Warrell DA (2010) Snake bite. *Lancet* 375: 77–88.
7. Sousa LF, Nicolau CA, Peixoto PS, Bernardoni JL, Oliveira SS, Portes-Junior JA, et al. (2013) Comparison of phylogeny, venom composition and neutralization by antivenom in diverse species of bothrops complex. *PLoS Negl Trop Dis* 7: e2442. doi: [10.1371/journal.pntd.0002442](https://doi.org/10.1371/journal.pntd.0002442) PMID: [24069493](https://pubmed.ncbi.nlm.nih.gov/24069493/)
8. Gutierrez JM, Lomonte B (1995) Phospholipase A₂ myotoxins from Bothrops snake venoms. *Toxicon* 33: 1405–1424. PMID: [8744981](https://pubmed.ncbi.nlm.nih.gov/8744981/)
9. Mebs D, Kuch U, Coronas FI, Batista CV, Gumprecht A, Possani LD (2006) Biochemical and biological activities of the venom of the Chinese pitviper *Zhafermia mangshanensis*, with the complete amino acid sequence and phylogenetic analysis of a novel Arg49 phospholipase A₂ myotoxin. *Toxicon* 47: 797–811. PMID: [16635500](https://pubmed.ncbi.nlm.nih.gov/16635500/)
10. Zhou X, Tan TC, Valiyaveetil S, Go ML, Kini RM, Velazquez-Campoy A, et al. (2008) Structural characterization of myotoxic ecarpholin S from *Echis carinatus* venom. *Biophys J* 95: 3366–3380. doi: [10.1529/biophysj.107.117747](https://doi.org/10.1529/biophysj.107.117747) PMID: [18586854](https://pubmed.ncbi.nlm.nih.gov/18586854/)
11. Arni RK, Ward RJ (1996) Phospholipase A₂—a structural review. *Toxicon* 34: 827–841. PMID: [8875770](https://pubmed.ncbi.nlm.nih.gov/8875770/)
12. Fernandes CA, Marchi-Salvador DP, Salvador GM, Silva MC, Costa TR, Soares AM, et al. (2010) Comparison between apo and complexed structures of bothropstoxin-I reveals the role of Lys122 and Ca(2+)-binding loop region for the catalytically inactive Lys49-PLA(2)s. *J Struct Biol* 171: 31–43. doi: [10.1016/j.jsb.2010.03.019](https://doi.org/10.1016/j.jsb.2010.03.019) PMID: [20371382](https://pubmed.ncbi.nlm.nih.gov/20371382/)
13. Lomonte B, Moreno E, Tarkowski A, Hanson LA, Maccarana M (1994) Neutralizing interaction between heparins and myotoxin II, a lysine 49 phospholipase A₂ from *Bothrops asper* snake venom. Identification of a heparin-binding and cytolytic toxin region by the use of synthetic peptides and molecular modeling. *J Biol Chem* 269: 29867–29873. PMID: [7961981](https://pubmed.ncbi.nlm.nih.gov/7961981/)
14. Nunez CE, Angulo Y, Lomonte B (2001) Identification of the myotoxic site of the Lys49 phospholipase A₂ from *Agkistrodon piscivorus piscivorus* snake venom: synthetic C-terminal peptides from Lys49, but not from Asp49 myotoxins, exert membrane-damaging activities. *Toxicon* 39: 1587–1594. PMID: [11478967](https://pubmed.ncbi.nlm.nih.gov/11478967/)
15. Ward RJ, Chioato L, de Oliveira AH, Ruller R, Sa JM (2002) Active-site mutagenesis of a Lys49-phospholipase A₂: biological and membrane-disrupting activities in the absence of catalysis. *Biochem J* 362: 89–96. PMID: [11829743](https://pubmed.ncbi.nlm.nih.gov/11829743/)
16. Chioato L, Aragao EA, Lopes Ferreira T, Medeiros AI, Faccioli LH, Ward RJ (2007) Mapping of the structural determinants of artificial and biological membrane damaging activities of a Lys49 phospholipase A₂ by scanning alanine mutagenesis. *Biochim Biophys Acta* 1768: 1247–1257. PMID: [17346668](https://pubmed.ncbi.nlm.nih.gov/17346668/)

17. Fernandes CA, Borges RJ, Lomonte B, Fontes MR (2014) A structure-based proposal for a comprehensive myotoxic mechanism of phospholipase A-like proteins from viperid snake venoms. *Biochim Biophys Acta* 1844: 2265–2276. doi: [10.1016/j.bbapap.2014.09.015](https://doi.org/10.1016/j.bbapap.2014.09.015) PMID: [25278377](https://pubmed.ncbi.nlm.nih.gov/25278377/)
18. Fernandes CA, Comparetti EJ, Borges RJ, Huancahuire-Vega S, Ponce-Soto LA, Marangoni S, et al. (2013) Structural bases for a complete myotoxic mechanism: crystal structures of two non-catalytic phospholipases A₂-like from Bothrops brazili venom. *Biochim Biophys Acta* 1834: 2772–2781. doi: [10.1016/j.bbapap.2013.10.009](https://doi.org/10.1016/j.bbapap.2013.10.009) PMID: [24145104](https://pubmed.ncbi.nlm.nih.gov/24145104/)
19. Soares AM, Ticli FK, Marcussi S, Lourenco MV, Januario AH, Sampaio SV, et al. (2005) Medicinal plants with inhibitory properties against snake venoms. *Curr Med Chem* 12: 2625–2641. PMID: [16248818](https://pubmed.ncbi.nlm.nih.gov/16248818/)
20. Samy RP, Thwin MM, Gopalakrishnakone P, Ignacimuthu S (2008) Ethnobotanical survey of folk plants for the treatment of snakebites in Southern part of Tamilnadu, India. *J Ethnopharmacol* 115: 302–312. PMID: [18055146](https://pubmed.ncbi.nlm.nih.gov/18055146/)
21. Mors WB, Nascimento MC, Pereira BM, Pereira NA (2000) Plant natural products active against snake bite—the molecular approach. *Phytochemistry* 55: 627–642. PMID: [11130675](https://pubmed.ncbi.nlm.nih.gov/11130675/)
22. Ticli FK, Hage LI, Cambraia RS, Pereira PS, Magro AJ, Fontes MR, et al. (2005) Rosmarinic acid, a new snake venom phospholipase A₂ inhibitor from Cordia verbenacea (Boraginaceae): antiserum action potentiation and molecular interaction. *Toxicon* 46: 318–327. PMID: [15992846](https://pubmed.ncbi.nlm.nih.gov/15992846/)
23. Cintra-Francischinelli M, Silva MG, Andreo-Filho N, Gerenutti M, Cintra AC, Giglio JR, et al. (2008) Anti-bothropic action of Casearia sylvestris Sw. (Flacourtiaceae) extracts. *Phytother Res* 22: 784–790. doi: [10.1002/ptr.2365](https://doi.org/10.1002/ptr.2365) PMID: [18389489](https://pubmed.ncbi.nlm.nih.gov/18389489/)
24. Vishwanath BS, Kini RM, Gowda TV (1987) Characterization of three edema-inducing phospholipase A₂ enzymes from habu (Trimeresurus flavoviridis) venom and their interaction with the alkaloid aristolochic acid. *Toxicon* 25: 501–515. PMID: [3617087](https://pubmed.ncbi.nlm.nih.gov/3617087/)
25. Vishwanath BS, Gowda TV (1987) Interaction of aristolochic acid with Vipera russelli phospholipase A₂: its effect on enzymatic and pathological activities. *Toxicon* 25: 929–937. PMID: [3433304](https://pubmed.ncbi.nlm.nih.gov/3433304/)
26. Vishwanath BS, Appu Rao AG, Gowda TV (1987) Interaction of phospholipase A₂ from Vipera russelli venom with aristolochic acid: a circular dichroism study. *Toxicon* 25: 939–946. PMID: [3433305](https://pubmed.ncbi.nlm.nih.gov/3433305/)
27. Chandra V, Jasti J, Kaur P, Srinivasan A, Betzel C, Singh TP (2002) Structural basis of phospholipase A₂ inhibition for the synthesis of prostaglandins by the plant alkaloid aristolochic acid from a 1.7 Å crystal structure. *Biochemistry* 41: 10914–10919. PMID: [12206661](https://pubmed.ncbi.nlm.nih.gov/12206661/)
28. Rice-Evans C, Miller N, Paganga G (1997) Antioxidant properties of phenolic compounds. *Trends in Plant Science* 2: 152–159.
29. Xie Y, Huang B, Yu K, Shi F, Liu T, et al. (2013) Caffeic acid derivatives: a new type of influenza neuraminidase inhibitors. *Bioorg Med Chem Lett* 23: 3556–3560. doi: [10.1016/j.bmcl.2013.04.033](https://doi.org/10.1016/j.bmcl.2013.04.033) PMID: [23664211](https://pubmed.ncbi.nlm.nih.gov/23664211/)
30. Huang MT, Smart RC, Wong CQ, Conney AH (1988) Inhibitory effect of curcumin, chlorogenic acid, caffeic acid, and ferulic acid on tumor promotion in mouse skin by 12-O-tetradecanoylphorbol-13-acetate. *Cancer Res* 48: 5941–5946. PMID: [3139287](https://pubmed.ncbi.nlm.nih.gov/3139287/)
31. Agoro JW (1978) Crystalline caffeic acid derivatives and compositions and method for treating snakebite. US 4124724 A.
32. Mancuso LC, Correa MM, Vieira CA, Cunha OA, Lachat JJ, de Araujo HS, et al. (1995) Fractionation of Bothrops pirajai snake venom: isolation and characterization of piratoxin-I, a new myotoxic protein. *Toxicon* 33: 615–626. PMID: [7660366](https://pubmed.ncbi.nlm.nih.gov/7660366/)
33. Bancroft JD, Stevens A (1990) Theory and practice of histological techniques. Edinburgh: Churchill Livingstone.
34. McPherson A (2003) Introduction to Macromolecular Crystallography. Hoboken: Wiley.
35. dos Santos JI, Soares AM, Fontes MR (2009) Comparative structural studies on Lys49-phospholipases A₂(2) from Bothrops genus reveal their myotoxic site. *J Struct Biol* 167: 106–116. doi: [10.1016/j.jsb.2009.04.003](https://doi.org/10.1016/j.jsb.2009.04.003) PMID: [19401234](https://pubmed.ncbi.nlm.nih.gov/19401234/)
36. Shimabuku PS, Fernandes CA, Magro AJ, Costa TR, Soares AM, Fontes MR (2011) Crystallization and preliminary X-ray diffraction analysis of a Lys49-phospholipase A₂ complexed with caffeic acid, a molecule with inhibitory properties against snake venoms. *Acta Crystallogr Sect F Struct Biol Cryst Commun* 67: 249–252. doi: [10.1107/S17443091110051407](https://doi.org/10.1107/S17443091110051407) PMID: [21301098](https://pubmed.ncbi.nlm.nih.gov/21301098/)
37. Otwinowski Z, Minor W (1997) Processing of X-ray Diffraction Data Collected in Oscillation Mode In: Carter CW Jr, Sweet RM, editors. *Macromolecular Crystallography part A*. New York: Academic Press. pp. 307–326.
38. Vagin A, Teplyakov A (1997) MOLREP: an automated program for molecular replacement. *Journal of Applied Crystallography* 30: 1022–1025.

39. Collaborative Computational Project N (1994) The CCP4 suite: programs for protein crystallography. *Acta Crystallogr D Biol Crystallogr* 50: 760–763. PMID: [15299374](#)
40. Emsley P, Lohkamp B, Scott WG, Cowtan K (2010) Features and development of Coot. *Acta Crystallogr D Biol Crystallogr* 66: 486–501. doi: [10.1107/S0907444910007493](#) PMID: [20383002](#)
41. Brunger AT, Adams PD, Clore GM, DeLano WL, Gros P, et al. (1998) Crystallography & NMR system: A new software suite for macromolecular structure determination. *Acta Crystallogr D Biol Crystallogr* 54: 905–921. PMID: [9757107](#)
42. Adams PD, Afonine PV, Bunkoczi G, Chen VB, Davis IW, Echols N, et al. (2010) PHENIX: a comprehensive Python-based system for macromolecular structure solution. *Acta Crystallogr D Biol Crystallogr* 66: 213–221. doi: [10.1107/S0907444909052925](#) PMID: [20124702](#)
43. Chen VB, Arendall WB III, Headd JJ, Keedy DA, Immormino RM, Kapral GJ, et al. (2010) MolProbity: all-atom structure validation for macromolecular crystallography. *Acta Crystallogr D Biol Crystallogr* 66: 12–21. doi: [10.1107/S0907444909042073](#) PMID: [20057044](#)
44. Schaloske RH, Dennis EA (2006) The phospholipase A₂ superfamily and its group numbering system. *Biochim Biophys Acta* 1761: 1246–1259. PMID: [16973413](#)
45. Magro AJ, Fernandes CA, dos Santos JI, Fontes MR (2009) Influence of quaternary conformation on the biological activities of the Asp49-phospholipases A₂s from snake venoms. *Protein Pept Lett* 16: 852–859. PMID: [19689411](#)
46. Salvador GH, Fernandes CA, Magro AJ, Marchi-Salvador DP, Cavalcante WL, Fernandez RM, et al. (2013) Structural and phylogenetic studies with MjTX-I reveal a multi-oligomeric toxin—a novel feature in Lys49-PLA₂s protein class. *PLoS One* 8: e60610. doi: [10.1371/journal.pone.0060610](#) PMID: [23573271](#)
47. dos Santos JI, Cardoso FF, Soares AM, Dal Pai Silva M, Gallacci M, Fontes MR (2011) Structural and functional studies of a bothropic myotoxin complexed to rosmarinic acid: new insights into Lys49-PLA₂ (2) inhibition. *PLoS One* 6: e28521. doi: [10.1371/journal.pone.0028521](#) PMID: [22205953](#)
48. Salvador GH, Cavalcante WL, Dos Santos JI, Gallacci M, Soares AM, Fontes MR (2013) Structural and functional studies with myotoxin II from Bothrops moojeni reveal remarkable similarities and differences compared to other catalytically inactive phospholipases A₂(2)-like. *Toxicon* 72: 52–63. doi: [10.1016/j.toxicon.2013.06.013](#) PMID: [23810946](#)
49. Cavalcante WL, Campos TO, Dal Pai-Silva M, Pereira PS, Oliveira CZ, Soares AM, et al. (2007) Neutralization of snake venom phospholipase A₂ toxins by aqueous extract of *Casearia sylvestris* (Flacourtiaceae) in mouse neuromuscular preparation. *J Ethnopharmacol* 112: 490–497. PMID: [17540522](#)
50. Gallacci M, Cavalcante WL (2010) Understanding the in vitro neuromuscular activity of snake venom Lys49 phospholipase A₂ homologues. *Toxicon* 55: 1–11. doi: [10.1016/j.toxicon.2009.10.025](#) PMID: [19874839](#)
51. Rodrigues-Simioni L, Borgese N, Ceccarelli B (1983) The effects of Bothrops jararacussu venom and its components on frog nerve-muscle preparation. *Neuroscience* 10: 475–489. PMID: [6605493](#)
52. Ownby CL, Selistre de Araujo HS, White SP, Fletcher JE (1999) Lysine 49 phospholipase A₂ proteins. *Toxicon* 37: 411–445. PMID: [10080349](#)
53. Montecucco C, Gutierrez JM, Lomonte B (2008) Cellular pathology induced by snake venom phospholipase A₂ myotoxins and neurotoxins: common aspects of their mechanisms of action. *Cell Mol Life Sci* 65: 2897–2912. doi: [10.1007/s00018-008-8113-3](#) PMID: [18563294](#)
54. Bowman WC, Rand MJ (1980) Striated Muscle and Neuromuscular Transmission In: Bowman W.C. R MJ, editor. *Textbook of Pharmacology*. Oxford: Blackwell Scientific Publications. pp. 17.11–17.56.
55. Correia-de-Sa P, Noronha-Matos JB, Timoteo MA, Ferreirinha F, Marques P, Soares AM, et al. (2013) Bothropstoxin-I reduces evoked acetylcholine release from rat motor nerve terminals: radiochemical and real-time video-microscopy studies. *Toxicon* 61: 16–25. doi: [10.1016/j.toxicon.2012.10.014](#) PMID: [23142504](#)
56. Johnson EK, Ownby CL (1994) The role of extracellular ions in the pathogenesis of myonecrosis induced by a myotoxin isolated from Broad-Banded copperhead (*Agkistrodon contortrix laticinctus*) venom. *Comp Biochem Physiol Pharmacol Toxicol Endocrinol* 107: 359–366. PMID: [8061942](#)
57. Gutierrez JM, Ownby CL (2003) Skeletal muscle degeneration induced by venom phospholipases A₂: insights into the mechanisms of local and systemic myotoxicity. *Toxicon* 42: 915–931. PMID: [15019491](#)
58. Bahnson BJ (2005) Structure, function and interfacial allostereism in phospholipase A₂: insight from the anion-assisted dimer. *Arch Biochem Biophys* 433: 96–106. PMID: [15581569](#)
59. Marchi-Salvador DP, Fernandes CA, Silveira LB, Soares AM, Fontes MR (2009) Crystal structure of a phospholipase A₂(2) homolog complexed with p-bromophenacyl bromide reveals important structural

changes associated with the inhibition of myotoxic activity. *Biochim Biophys Acta* 1794: 1583–1590. doi: [10.1016/j.bbapap.2009.07.005](https://doi.org/10.1016/j.bbapap.2009.07.005) PMID: [19616648](https://pubmed.ncbi.nlm.nih.gov/19616648/)

60. Laskowski RA, Swindells MB (2011) LigPlot+: multiple ligand-protein interaction diagrams for drug discovery. *J Chem Inf Model* 51: 2778–2786. doi: [10.1021/ci200227u](https://doi.org/10.1021/ci200227u) PMID: [21919503](https://pubmed.ncbi.nlm.nih.gov/21919503/)